Journal of Organometallic Chemistry 693 (2008) 3263–3272

Contents lists available at ScienceDirect

Journal of Organometallic Chemistry

journal homepage: www.elsevier.com/locate/jorganchem

1,4-Bis(phosphine)-2,5-difluoro-3,6-dihydroxybenzenes and their P-oxides: Syntheses, structures, ligating and electronic properties

Louis R. Pignotti [a], Natcharee Kongprakaiwoot [a], William W. Brennessel [b], Jonas Baltrusaitis [c], Rudy L. Luck [a], Eugenijus Urnezius [a,*]

[a] Department of Chemistry, Michigan Technological University, 1400 Townsend Dr, Houghton, MI 49931, United States
[b] Department of Chemistry, University of Rochester, B51 Hutchinson Hall, 120 Trustee Road, Rochester, NY 14627, United States
[c] Department of Chemistry and Central Microscopy Research Facility, University of Iowa, 76 Eckstein Medical Research Building, Iowa City, IA 5224, United States

ARTICLE INFO

Article history:
Received 21 May 2008
Received in revised form 18 July 2008
Accepted 20 July 2008
Available online 29 July 2008

Keywords:
Noninnocent ligands
Binucleating
Structures
Electrochemistry
Frontier orbitals

ABSTRACT

Reactions of 1,4-difluoro-2,5-dimethoxybenzene with LDA (1:2) at low temperatures generated organodilithio intermediates; quenching the reaction mixtures with chlorophosphines $ClPR_2$ produced 1,4-bis(phosphino)-2,5-difluoro-3,6-dimethoxybenzenes **1a** (R = Ph) and **1b** (R = *i*Pr). Demethylation of **1a–b** was accomplished by BBr_3, yielding bis(phosphino)hydroquinones **2a–b**. Treating **2a–b** with excess hydrogen peroxide produced bis(phosphinyl)hydroquinones **3a–b**. The binucleating properties of **2a** were established by the formation of a bimetallic nickel complex upon reaction with $Ph_2Ni(PMe_3)_2$. Electrochemical activity of hydroquinones **2a–b** and **3a–b** was examined by cyclic voltammetry. In addition, compounds **2a**, **3a** and **3b** were obtained in crystalline form and characterized by single-crystal X-ray diffraction. The influence of the fluorine substituents on the composition of the frontier orbitals of **2a** and **3a** was examined by computational methods.

1. Introduction

Ligands containing *p*-quinone structural motifs are being increasingly utilized in the design and construction of bimetallic complexes and coordination polymers. Thus, simple *p*-quinone linkages have been successfully used in producing multimetallic assemblies containing early transition metals (Fig. 1A) [1–7]. Coordination networks where the *p*-quinoid fragments function both as σ- (O-ligation) and π-ligands (via coordination of another transition metal containing fragment onto the quinone ring) have also been extensively studied [8–11].

Polymetallic compounds possessing higher directionality and increased stability are often obtained if binucleating *p*-quinoid ligands contain chelation sites (Fig. 1B) are used. Most of the currently used ligands allowing for the formation of compounds B have either [O,O] (various dihydroxybenzoquinones [12]) or [O,N] (2,5-bis(pyrazol-1-yl)-1,4-dihydroxybenzene or related derivatives [13–19]) chelation pockets. Despite the extensive general usage of phosphine-based ligands in coordination chemistry, binucleating ligands based on the *p*-quinoid moiety appended by phosphine substituents (i.e., having [P,O] chelating pockets) have received only limited attention. To the best of our knowledge, only one bimetallic complex supported by a 2,5-bis(phosphino)-*p*-quinoid ligand has been reported [20]. The lack of broader interest in phosphine–quinoid ligands is most likely caused by their somewhat complicated synthetic procedures [20,21] and by the fact that such ligands can not be isolated in their oxidized (quinone) state. The latter complication arises from the facile reaction of phosphines with quinones [22], making the two moieties (phosphine and quinone) incompatible. However, phosphine–quinone ligands are readily isolable in their reduced (hydroquinone) form, and their degradation upon oxidation to quinone is prevented if the nucleophilicity of the phosphine moiety is neutralized by tying up the lone pair of electrons on phosphorus in bonding [21,23–26].

Coordination polymers containing metal centers embedded directly into the main chains of the macromolecules are actively pursued as potentially highly tunable novel materials [27,28]. The presence of linked electroactive units (redox-active ligands and metal centers) in such compounds presents an attractive opportunity for developing molecular systems where numerous stimuli/response features can be utilized using chemical, electrical and optical methods. In particular, such compounds are being considered as potential molecular conductors and sensors [29]. While several of quinoid-based ligands have been explored for this purpose [30–33], the number of such ligands is still limited. Herein we present syntheses, structural and electrochemical investigations of new 2,5-bis(phosphino)-*p*-hydroquinones (Fig. 2, **2a–b**), their P-oxides (Fig. 2, **3a–b**), and initial studies of their ligation properties (Figs. 2, 5). Theoretical analyses of frontier molecular

* Corresponding author. Tel.: +1 906 487 2055; fax: 1 906 487 2061.
E-mail address: urnezius@mtu.edu (E. Urnezius).

0022-328X/$ - see front matter © 2008 Elsevier B.V. All rights reserved.
doi:10.1016/j.jorganchem.2008.07.023

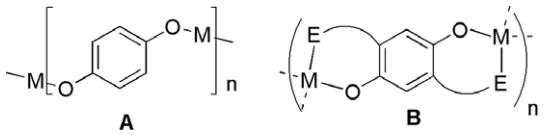

Fig. 1. General structural motifs of coordination polymers built on *p*-quinoid ligands. M = transition metal; E = donor atom (O, N, or P) positioned 1 or 2 bonds away from the central ring.

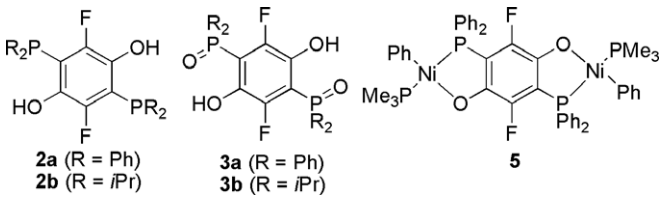

Fig. 2. New 2,5-bis(phosphino)- and 2,5-bis(phosphinyl)-hydroquinones, and bimetallic nickel complex.

orbitals of compounds **2a**–**3a** and their fluorine-free analogs, **2aH**–**3aH** are also presented and discussed.

2. Experimental

2.1. General procedures

Synthetic preparations and procedures were carried out by using suitably adapted Schlenk techniques or in a dry box under a N_2 atmosphere. Low temperature reactions were performed in Schlenk flasks immersed in ethanol/liquid N_2 slush, contained in a Dewar flask. Solvents were purified before use by distillation from Na-benzophenone ketyl (ether, THF, hexanes, benzene) or CaH_2 (toluene, 2-propanol, dichloromethane) or Na (pyridine) under a N_2 atmosphere. Dry methanol was obtained by distillation from $Mg(OCH_3)_2$ under a N_2 atmosphere. Deoxygenated methanol and ethanol were obtained by bubbling nitrogen through the solvent for 1 h. Commercially available chlorophosphines were purified prior to usage: $ClPPh_2$ was distilled under reduced pressure; $ClPiPr_2$ was frozen and degassed while thawing under vacuum (repeated 3 times). Lithium diisopropylamide (LDA) was freshly prepared immediately prior to use according to a published procedure [34]. Triethylamine was distilled from CaH_2 under nitrogen. Nickel complexes $NiCl_2(PMe_3)_2$ [35] and $Ph_2Ni(PMe_3)_2$ [36] were prepared utilizing literature procedures. ^1H, ^{13}C, ^{31}P, and ^{19}F NMR spectra were recorded on Varian INOVA spectrometer operating at 400, 100, 161, and 376 MHz, respectively. Spectra are referenced to tetramethylsilane (^1H and ^{13}C), 85% H_3PO_4 as an external reference (^{31}P), and $CFCl_3$ as an internal reference in a sealed capillary tube (^{19}F). Low resolution mass spectrometric measurements were performed on Shimadzu QP5050A instrument; high resolution mass spectrometric measurements were performed at Mass Spectrometry Facility at Michigan State University (East Lansing, MI 48824-1319). Elemental analyses were performed at Galbraith Laboratories Inc.

Electrochemical measurements (CV) were performed using a CHI420 electrochemical analyzer. A standard 3-electrode cell fitted to operate under air-tight conditions was used. A glassy carbon disk (3 mm), $Ag/AgNO_3$ and Pt wire were used as working, reference, and counter electrodes, respectively. Measurements for **2a**–**b** (scan rate of 0.5 V/s) and **3a**–**b** (scan rate 0.1 V/s) were performed in ~1 mM solutions in CH_2Cl_2 containing 0.1 M NBu_4PF_6 as supporting electrolyte.

2.2. Syntheses

2.2.1. 1,4-Bis(diphenylphosphino)-2,5-difluoro-3,6-dimethoxybenzene (*1a*)

To a cold (−95 °C) stirred solution of 1,4-difluoro-2,5-dimethoxybenzene (1.00 g, 5.74 mmol) in THF (120 mL) 2.0 equiv. of freshly prepared LDA (in THF, 20 mL) was added. After stirring the reaction mixture for 5 min at -95 °C, a solution of $ClPPh_2$ (2.5 equiv.) in THF (30 mL) was slowly (over 30 min) added. The mixture was stirred at −95 °C for 1 h and then allowed to slowly warm up while stirring overnight. The resulting solution was filtered, and all volatiles were removed under reduced pressure to yield a pale yellow solid. Washing it with hot deoxygenated methanol (100 mL) yielded **1a** as white powder. Yield: 2.329 g (74.8%). M.p.: 156–157 °C. ^1H NMR (acetone-d_6): δ 7.40 (m, 20H), 3.48 (s, 6H). ^{31}P NMR ($CDCl_3$): δ −20.4 (dd, $^3J_{PF}$ = 20 Hz, $^4J_{PF}$ = 9 Hz). ^{19}F NMR ($CDCl_3$): δ −120.1 (dd, $^3J_{FP}$ = 20 Hz, $^4J_{FP}$ = 9 Hz). HRMS (FAB): MH^+ Calc. for $C_{32}H_{27}F_2O_2P_2$: 543.1454. Found: 543.1456.

2.2.2. 1,4-Bis(diisopropylphosphino)-2,5-fluoro-3,6-dimethoxybenzene (*1b*)

The synthesis of **1b** was accomplished by employing $ClPiPr_2$ instead of $ClPPh_2$ in the procedure used for **1a**; 2.00 g (11.74 mmol) of 1,4-difluoro-2,5-dimethoxybenzene was used. The resulting light yellow solid was redissolved in hot deoxygenated methanol (70 mL), and light yellow crystals of **1b** precipitated on standing at −10 °C overnight. Yield: 2.934 g (62.9%). M.p.: 91–92 °C. ^1H NMR ($CDCl_3$): δ 3.84 (s, 6H, (OCH_3)), 2.48 (m, 4H, (PC*H*)), 1.14 (dd, 12H, $^3J_{PH}$ = 17 Hz, $^3J_{HH}$ = 7 Hz, (CH_3)), 0.92 (dd, 12H, $^3J_{PH}$ = 12 Hz, $^3J_{HH}$ = 7 Hz, (CH_3)). ^{13}C NMR ($CDCl_3$): δ 154.0 (dm, $^1J_{CF}$ = 244 Hz (*C*F)), 147.2 (m, C_{arom}-OCH_3), 121.9 (m (C_{arom}-P)), 62.0 (s (OCH_3)), 24.0 (d, $^1J_{PC}$ = 12 Hz ($PCH(CH_3)_2$)), 21.4 (d, $^2J_{PC}$ = 24 Hz (CH_3)), 20.9 (d, $^2J_{PC}$ = 11 Hz (CH_3)). ^{31}P NMR ($CDCl_3$): δ 4.8 (s, br). ^{19}F NMR ($CDCl_3$): δ −121.3 (s, br). HRMS (FAB): MH^+ Calc. for $C_{20}H_{35}F_2O_2P_2$: 407.2080. Found: 407.2081.

2.2.3. 1,4-Bis(diphenylphosphino)-2,5-difluoro-3,6-dihydroxybenzene (*2a*)

To a stirred solution of 1,4-bis(diphenylphosphino)-2,5-difluoro-3,6-dimethoxybenzene (**1a**; 1.00 g, 1.85 mmol) in 80 mL of dichloromethane at -80 °C BBr_3 (0.80 mL, 8.49 mmol) was added. The mixture was stirred at -80 °C for 10 min and then allowed to warm up to room temperature overnight. Volatiles were removed under reduced pressure to yield a white solid which was subsequently treated with dry methanol (30 mL) at 0 °C. The resulting suspension was removed from the cooling bath and then was stirred at room temperature overnight. All volatiles were removed in vacuo, and 2-propanol (50 mL) and NEt_3 (1.20 mL, 8.49 mmol) were added to the remaining solid. After 2 h of stirring, the mixture was filtered leaving a light yellow solid which was redissolved in 40 mL of a 1:1 mixture of pyridine and 2-propanol. Yellow crystals of **2a**·$2C_5H_5N$ (suitable for X-ray analysis) were formed after the solution was kept at −28 °C for 2 days; a second fraction of crystals was collected from the mother liquor after ten days at −28 °C. Total yield: 0.646 g (68.1%). M.p.: 233–234 °C. ^1H NMR ($CDCl_3$): δ 7.45 (m, 8H), 7.35 (m, 12H). ^{31}P NMR ($CDCl_3$): δ −30.6 (m). ^{19}F NMR (pyridine-d_5): δ −125.5 (dd, $^3J_{FP}$ = 18 Hz, $^4J_{FP}$ = 10 Hz). HRMS (FAB): MH^+ Calc. for $C_{30}H_{23}F_2O_2P_2$: 515.1141. Found: 515.1139.

2.2.4. 1,4-Bis(diisopropylphosphino)-2,5-difluoro-3,6-dihydroxybenzene (*2b*)

A solution of 1,4-bis(diisopropylphosphino)-2,5-difluoro-3,6-dimethoxybenzene (**1b**; 3.30 g, 8.2 mmol) in CH_2Cl_2 (200 mL) was cooled to −80 °C and BBr_3 (3.9 mL, 41 mmol) was added. The reaction mixture was stirred overnight while slowly attaining room temperature. All volatiles were removed under reduced pres-

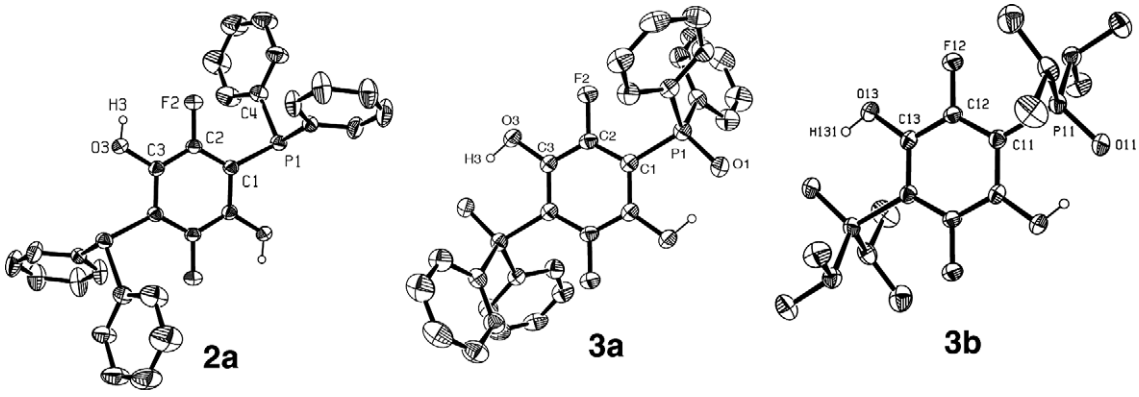

Fig. 3. Thermal ellipsoid plots (30%) of **2a**, **3a** and **3b**.

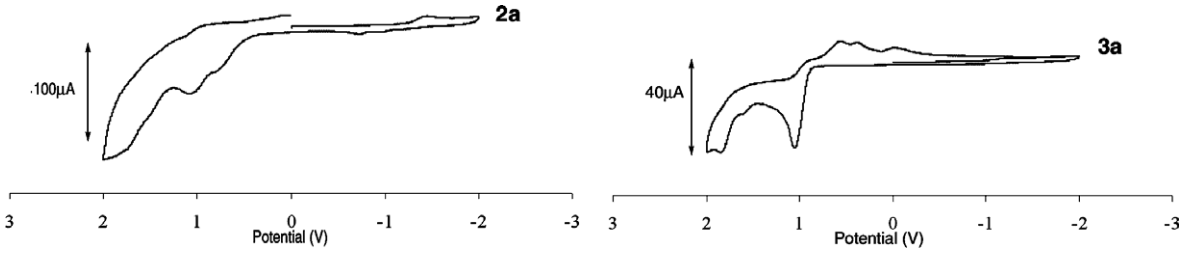

Fig. 4. Cyclic voltammetry plots of **2a** and **3a**.

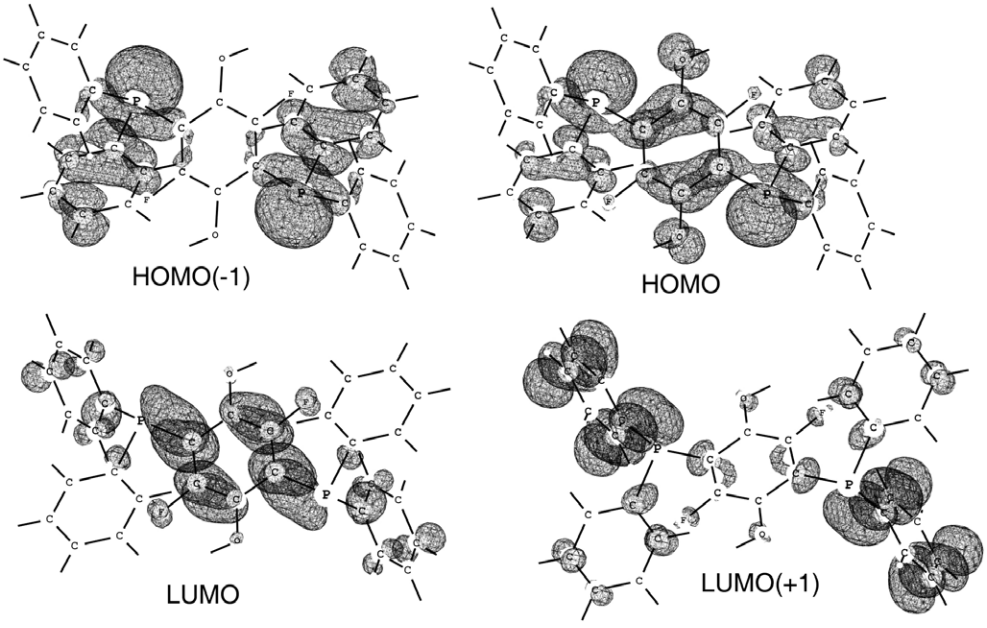

Fig. 5. Frontier orbitals (contour plots) of **2a**.

sure, the flask was cooled in an ice bath, and 50 mL of methanol was added to the residual solid. The resulting slurry was stirred overnight while attaining room temperature. All volatiles were removed under reduced pressure, followed by addition (at 0 °C) of 2-propanol (100 mL) and triethylamine (5.4 mL, 38.4 mmol). After stirring for 2 days at room temperature all the volatiles were removed under reduced pressure and THF (100 mL) was added. The resulting slurry was then filtered, all volatiles were removed under vacuum, and the remaining pale orange solid was washed with two 60 mL portions of diethyl ether. Yield: 1.862 g (59.8%). M.p.: 216–218 °C. ^{1}H NMR ($CDCl_3$): δ 6.68 (s (br), 2H (O*H*)), 2.53 (m, 4H (PC*H*)), 1.16 (dd, 12H, $^{3}J_{PH}$ = 18 Hz, $^{3}J_{HH}$ = 7 Hz (*CH*$_3$)), 0.94 (dd, 12H, $^{3}J_{PH}$ = 14 Hz, $^{3}J_{HH}$ = 7 Hz). ^{13}C NMR ($CDCl_3$): δ 148.1 (dm, $^{1}J_{CF}$ = 240 Hz, *C*F), 140.8 (m, *C*OH), 113.3 (m, C_{arom}P), 23.4 (s, (CH)), 21.2 (d, $^{2}J_{CP}$ = 21 Hz (*CH*$_3$), 20.5 (d, $^{2}J_{CP}$ = 20 Hz, (*CH*$_3$)). ^{31}P NMR ($CDCl_3$): δ −11.7 (m). ^{19}F NMR (pyridine-d_5): δ −127.9 (dd, $^{3}J_{FP}$ = 47 Hz, $^{4}J_{FP}$ = 9 Hz). HRMS (FAB): MH^+ Calc. for $C_{18}H_{31}F_2O_2P_2$: 379.1767. Found: 379.1766.

2.2.5. 1,4-Bis(diphenylphosphinyl)-2,5-difluoro-3,6-dihydroxybenzene (**3a**)

(*Caution!* Acetone/H_2O_2 mixtures can form explosive products. Protecting shields and other necessary safety measures should be used.) Hydrogen peroxide (5 mL, 30% in H_2O) was added to a solution of 1,4-bis(diphenylphosphino)-2,5-difluoro-1,4-dihydroxybenzene (**2a**; 0.836 g, 1.6 mmol) in 70 mL of acetone. The solution was allowed to stir overnight. Subsequent filtration/drying in vacuo yielded 0.558 g of a fine white powder **3a**. An additional 0.150 g of **3a** was recovered after the volume of the filtrate was reduced to 50 mL followed by cooling to −28 °C for several days. Combined yield: 0.708 g (81.0%). M.p.: 275–277 °C. ^{1}H NMR ($CDCl_3$): δ 7.79 (m, 8H), 7.62 (m, 4H), 7.51 (m, 8H). ^{31}P NMR ($CDCl_3$): δ 42.2 (s). ^{19}F NMR (acetone): δ −125.2 (s (br)). HRMS (FAB): MH^+ Calc. for $C_{30}H_{23}F_2O_4P_2$: 547.1040. Found: 547.1035.

2.2.6. 1,4-Bis(diisopropylphosphinyl)-2,5-difluoro-3,6-dihydroxybenzene (**3b**)

To a stirring solution of 1,4-bis(diisopropylphosphino)-2,5-difluoro-3,6-dihydroxybenzene (**2b**; 0.563 g, 1.49 mmol) in 20 mL of acetone was added 0.75 mL of 30% H_2O_2 (5 equiv.). The solution turned clear dark orange as it was allowed to stir overnight. Removing all volatiles in vacuo yielded 0.569 g of a pale orange solid **3b** (>90% pure by NMR; crude yield ~90%). Further purification can be performed by crystallizations from diethyl ether/acetone (1:1, −28 °C, 4–5 days) or methanol (−28 °C, 4–5 days), producing **3b** in the form of white crystalline substance in ~70% yield. M.p.: 193–196 °C. ^{1}H NMR ($CDCl_3$): δ 11.82 (s, 2H (O*H*)), 2.41 (m, 4H(CH)), 1.29 (dd, 12H, $^3J_{CP}$ = 17 Hz, $^3J_{HH}$ = 7 Hz (CH_3)), 1.17 (dd, 12H, $^3J_{CP}$ = 18 Hz, $^3J_{HH}$ = 7 Hz (CH_3)). ^{13}C NMR ($CDCl_3$): δ 145.3 (dm, $^1J_{CF}$ = 241 Hz, (C*F*)), 143.4 (m (C*O*H)), 105.7 (dm, $^1J_{CP}$ = 74 Hz (C_{arom}P)), 27.8 (d, $^1J_{CP}$ = 66 Hz (P*C*H)), 16.2 (s (br), (*C*H$_3$)), 14.9 (s (br), (CH$_3$)). ^{31}P NMR ($CDCl_3$): δ 72.8 (s). ^{19}F NMR ($CDCl_3$): δ −129.5 (s (br)). HRMS (FAB): MH^+ Calc. for $C_{18}H_{31}F_2O_4P_2$: 411.1666. Found: 411.1669.

2.2.7. [Ph(PMe$_3$)Ni-(P,O)-μ{(1,4-(PPh$_2$)$_2$-2,5-F$_2$-3,6-O$_2$-C$_6$)}-(P,O)-Ni(PMe$_3$)Ph] (**5**)

A solution of **2a** (0.246 g, 0.479 mmol) in 20 mL of THF was slowly added to a solution of $Ph_2Ni(PMe_3)_2$ (0.35 g, 0.959 mmol) in 20 mL of THF. The reaction mixture was heated at reflux for 4 h, followed by the removal of all volatiles under reduced pressure. The remaining yellow solid **5** was washed with 10 mL of toluene. Yield: 0.262 g (58.4%). ^{1}H NMR (C_6D_6): δ 7.10 (m, 30H), 2.14 (s (br), 9H). ^{31}P NMR: δ 24.9 (dm, $^2J_{PP}$ = 309 Hz, *P*Ph$_2$), −12.8 (dm, $^2J_{PP}$ = 309 Hz, *P*Me$_3$). ^{19}F NMR: δ −130.3 (d, $^3J_{FP}$ = 36 Hz). Anal. Calc. for $C_{48}H_{48}F_2Ni_2O_2P_4$: C, 61.58; H, 5.17. Found: C, 60.91; H, 4.96% (repeated elemental analyses were consistently slightly low on carbon).

2.2.8. NiCl$_2$(PMe$_3$)$_2$

A solution of PMe_3 (16.8 mL, 1.0 M in THF) was added to a stirred solution of $NiCl_2 \cdot 6H_2O$ (2.00 g, 8.41 mmol in 30 mL of deoxygenated ethanol), yielding a dark red solution immediately. After stirring the reaction mixture overnight, volatiles were removed under vacuo to give a red solid which was redissolved in 30 mL of warm ethanol. The solution was cooled in an ice bath for 1 h, resulting in the formation of dark red crystals which were isolated by filtration. A second fraction of crystals was obtained after the filtrate was kept at −28 °C for 2 weeks. Yield (~55%) and m.p. (201–202 °C) matched the reported values [35] well.

2.3. X-ray crystallography

Compound **2a** was analyzed at the X-ray crystallographic facility, at the University of Rochester. A crystal was placed onto the tip of a 0.1 mm diameter glass fiber and mounted on a Bruker SMART APEX II CCD diffractometer for data collection at 243.0(2) K. Attempts at lower temperatures resulted in multiply twinned data, suggesting that the crystals suffered from thermal stress. A preliminary set of cell constants and an orientation matrix were calculated from 385 reflections harvested from three sets of 20 frames. These initial sets of frames were oriented such that orthogonal wedges of reciprocal space were surveyed. The data collection was carried out using Mo Kα radiation with a frame time of 30 s and a detector distance of 5.02 cm. A randomly oriented region of reciprocal space was surveyed: four major sections of frames were collected with 0.50° steps in ω at four different φ settings and a detector position of −33° in 2θ. The intensity data were corrected for absorption [37]. Final cell constants were calculated from the *xyz* centroids of 3107 strong reflections from the actual data collection after integration [38]. The space group $P2_1/n$ was determined based on systematic absences and intensity statistics. A direct-methods solution was calculated using SIR97 [39] which provided most non-hydrogen atoms from the E-map. Full-matrix least squares/differences Fourier cycles were performed using SHELXL-97 [40] which located the remaining non-hydrogen atoms. All non-hydrogen atoms were refined with anisotropic displacement parameters. The hydrogen atom of the OH group was found from the difference map, and then was refined positionally and thermally with respect to the oxygen atom. All other hydrogen atoms were placed in ideal positions and refined as riding atoms with relative isotropic displacement parameters.

Compounds **3a**–**b** were characterized using crystal preparation, data collection and refinement procedures described in our previous reports [41]. Crystals of **3a**–**b** suitable for X-ray analysis were obtained by crystallization from methanol solutions. In **3a**–**b**, the hydrogen atom of the OH group was freely refined resulting in O-H distances of 0.91(3), 0.83(3) and 0.82(3) Å and U_{ISO} values for the H atom of 0.083(9), 0.064(9) and 0.062(9) for **3a** and the two independent molecules of **3b,** respectively. In both cases the remaining H atoms were refined as described above for **2a**.

2.4. Calculations

Density functional theory (DFT) calculations were performed using GAUSSIAN 03 software package revision B.01 [42]. Geometries were optimized using spin restricted calculations with B3LYP exchange correlation functional and 6-31G(d) basis set as implemented in GAUSSIAN 03 [43,44]. All stationary points were verified as minima using vibrational frequency calculations at the same level of theory. Tight convergence cutoffs were used in geometry optimization calculations. Additional single point calculations were performed at B3LYP/6-31G(d) geometry using R3BLYP exchange correlation functional with TZVP basis set [45]. Molecular orbital (MO) compositions were calculated using AOMix [46,47] software package and the Mulliken scheme [48–51]. Molecular orbitals were visualized using Chemcraft software package [52].

3. Results and discussion

3.1. Syntheses

Recently we reported on the preparation of several new polydentate phosphine [41,53] and mixed donor [P,S] [54] ligands. The synthetic method utilized in such syntheses relies on the sequential generation of organodilithio intermediates from selected tetrasubstituted benzenes. In particular, low temperature (−95 °C) double deprotonation of 1,4-dibromo-2,5-difluorobenzene [53,54], 1,2-dibromo-4,5-difluorobenzene [41], or 1-bromo-2-chloro-4,5-difluorobenzene [41] with lithium diisopropylamide

(LDA) was possible due to the relative acidity of the aromatic protons flanked by F/Br or F/Cl substituents on the same phenyl ring. Alkoxy groups are known to direct *ortho*-lithiations on the phenyl rings, including the dilithiations of some ethers [55]. Not surprisingly, double deprotonation at the CH_3O/F flanked aromatic positions and the formation of organodilithium intermediate (Eq. (1), step 1) are facile

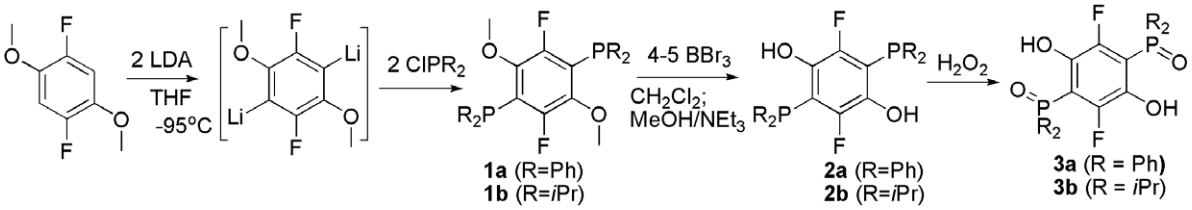

(1)

when 1,4-difluoro-2,5-dimethoxybenzene is reacted with LDA (2 equivalents), as judged by the relatively high isolated yields (>60%) of 1,4-bis(phosphino)-2,5-difluoro-3,6-dimethoxybenzenes **1a**–**b** (Eq. (1)). Similar *p*-dialkoxybenzenes appended with phosphine groups at the 2- and 5-positions have been known for some time [56]. Compounds **1a**–**b** represent methyl-protected forms of highly substituted 1,4-hydroquinones. They are white/pale yellow crystalline solids that are stable to oxidation when handled in air. Conversion of **1a**–**b** into the corresponding hydroquinones **2a**–**b** is relatively facile using BBr_3 as the O-dealkylating reagent, as such procedures are typical for analogous dealkylations producing *o*-phosphinophenols [21,57]. Compound **2b** is isolated in lower yield, most likely due to the higher stability of phosphonium salts (**2b**·*n*HBr) formed by protonation of more basic diisopropylphosphino groups during the dealkylation procedure [21,57]. Solution ^{31}P NMR data for compounds **2a** (δ −30.6) and **2b** (δ −11.7) resemble chemical shift values reported for *o*-diphenylphosphinophenols ($\delta \sim -26$) [58,59] and *o*-diisopropylphosphinophenols ($\delta \sim -22$) [60].

Phosphorus centers in hydroquinones **2a**–**b** are only moderately sensitive to oxidation by atmospheric oxygen. Thus, the presence of P-oxide **3a** (^{31}P NMR δ 42.2) was evident after about 48 h of exposure of a solution of **2a** in $CDCl_3$ to air. Continued monitoring of the relative **2a**/**3a** signal intensities in the ^{31}P NMR spectrum revealed that approximate 50% conversion of **2a** into **3a** was achieved after 4 weeks. The final spectrum also contained small (<10%) quantities of species with δ values of 39.0 and −31.7, which we assigned to a product of partial oxidation of **2a** (Ph_2-P-$C_6(OH)_2F_2$-P(O)Ph_2) (also verified by the presence of strong peak at $m/z = 530$ (M^+) in mass-spectrometric measurements of the reaction mixture). Similar reactivity pattern was also observed for phosphorus centers in **2b**. Such relative stability of **2a**–**b** to P-oxidation is quite surprising, given the fact that *o*-phosphinophenols typically are quite air sensitive [61] and some of them form P-oxides almost instantly upon exposure to air [57,62]. Detailed investigations addressing the oxidation of phosphorus centers in *o*-phosphinophenols and in phosphine-appended hydroquinones are currently unavailable. Our theoretical investigations (discussed in Section 3.4.) suggest that such behavior of **2a**–**b** towards O_2 may be attributed to the presence of fluorine substituents on the central phenyl ring as they have a direct influence on the composition of the HOMO in **2a**.

Oxidation of the P centers in **2a**–**b** is facile when excess of 30% H_2O_2 is used as an oxidizing reagent (Eq. (1), last step); the phosphine oxides **3a**–**b** conveniently precipitate out of the reaction mixture. They are white, crystalline solids, soluble in polar organic solvents (particularly in alcohols). Our attempts to further oxidize hydroquinones **3a**–**b** into corresponding quinones have not been successful so far (oxidizing reagents used: $[Cp_2Fe]PF_6$, $NaIO_4$, $Ce(NH_4)_2(NO_3)_6$, potassium nitrosodisulfonate, and others).

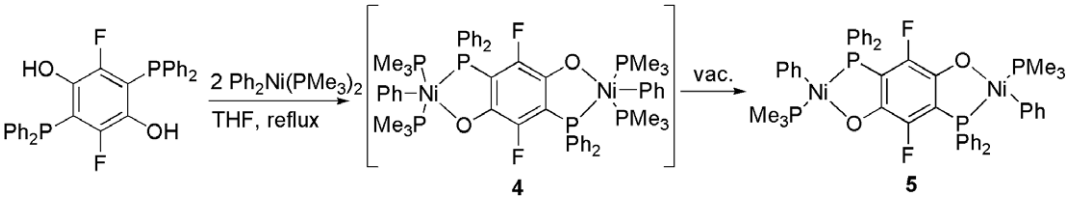

(2)

We have started investigating the ligating properties of **2a**–**b** and **3a**–**b**. Our preliminary results suggest that compound **2a** functions as an effective binucleating ligand as judged by the formation of organometallic nickel complexes **4** and **5** (Eq. (2)). When heated, a THF solution of **2a** and $Ph_2Ni(PMe_3)_2$ (1:2 ratio) slowly (hours) changes color from deep red to orange to yellow. The progress of the reaction monitored by ^{31}P NMR can be assessed by the disappearance of signals for the starting nickel complex ($Ph_2Ni(PMe_3)_2$, δ −10.8) and for ligand **2a**. A new set of signals seen in the spectrum (δ 24.7 (br), −40.7 (br)) is attributed to the formation of bimetallic complex **4** (Eq. (2)) (not isolated). This assignment is based on a comparison of the spectral signature of **4** to the signals observed for similar monometallic *o*-phosphinophenolate methylnickel-(bis)trimethylphosphine complex (δ 27.0 (br), −28.5(br)) [60], where the broadness of the signals is attributed to the fluxional behavior of the PMe_3 ligands at the formally pentacoordinate nickel center [36]. The lability of the PMe_3 ligands in **4** is also illustrated by the fact that removing the volatiles in vacuo during the reaction workup produces bimetallic complex **5** (yellow powder) (Eq. (2)) where only one PMe_3 ligand is coordinated to four-coordinate nickel center. Despite numerous attempts we have not been

able to obtain single crystals of **5** suitable for crystallographic investigations. The strongest evidence of the assignment of **5** as a bimetallic quinonate complex comes from a comparison of its ^{31}P NMR spectral signature (δ 24.9 (dm, $^2J_{PP}$ = 309 Hz, $P\text{Ph}_2$), −12.8 (dm, $^2J_{PP}$ = 309 Hz, $P\text{Me}_3$)) to those of monometallic organonickel trimethylphosphine *o*-phosphinophenolates, where a large value for $^2J_{PP}$ is indicative for the *trans* arrangement of the two phosphorus centers. The complex phenylnickel-2-(diphenylphosphino)phenolate(O,P)(trimethylphosphine) displays very similar chemical shift (^{31}P NMR, δ 23.6 (d), −13.4 (d)) and coupling constant ($^2J_{PP}$ = 303 Hz) values in solution at −60 °C; broad signals are reported for the room temperature spectrum [36]. By contrast, we observed sharp signals in the spectra of **5** recorded at room temperature (with some multiplet character due to unresolved ^{19}F–^{31}P couplings). Differences in fluxional behavior (responsible for the broadening of NMR signals) among similar nickel [P,O] complexes have been noted before [36], but the reasons behind this phenomenon are not yet known.

3.2. Structural investigations

To the best of our knowledge, hydroquinones **2a**–**b** constitute the second and third examples of compounds having 1,4-bis(phosphino)-2,5-dihydroxybenzene motifs reported in the literature; data about 1,4-bis(phosphinyl)-2,5-dihydroxybenzenes analogous to **3a**–**b** are also quite limited [63]. Also, no structural characterizations of such compounds have been reported previously. We have obtained single crystals of **2a** and **3a**–**b** suitable for X-ray diffraction experiments, and determined their crystal and molecular structures (general crystallographic data are summarized in Table 1).

Thermal ellipsoid plots of hydroquinones **2a**, **3a** and **3b** are presented in Fig. 3, with selected bond distances and angles summarized in Table 2. Crystals of **2a** contain pyridine as a co-crystallized solvent. The molecule of hydroquinone **2a** lies on a crystallographic inversion center; thus, one half of the molecule is unique. The two disordered co-crystallized pyridine molecules (one unique) per hydroquinone molecule interact with the hydroxyl groups of **2a** through [-N···H–O–] hydrogen bonding (not shown in Fig. 3). Most of the bond distances and angles are unexceptional. The oxygen and fluorine substituents are in the plane of the central phenyl ring, while phosphorus atom P1 is displaced from it by 0.129 Å. The –PPh_2 group in **2a** is rotated around the C1–P1 bond so that one of the Ph substituents has the plane of the aromatic ring directly facing the fluorine on the central phenyl ring. This is illustrated by the F2–C4 distance of 2.86 Å, which is substantially shorter then the sum of van der Waals radii for C and F, estimated around 3.05 Å [64]. The proximity of F2 and C4 is also most likely responsible for the relatively large C2–C1–P1 angle (126.99(10)°). We have previously observed similar arrangements of the –PPh_2 groups attached to the phenyl ring containing fluorine substituents at *ortho* positions [41]; the underlying reasons for these apparent C–F interactions in **2a** are unclear at the moment.

Crystals of **3a** and of **3b** do not contain co-crystallized solvent. Two independent molecules comprising the unit cell of **3b** have very small differences, thus only one of them is shown in Fig. 3 and discussed. The oxygen atoms from the phosphinyl groups in **3a**–**b** are engaged in hydrogen bonding with the protons from the OH groups of the hydroquinone, which is a common feature for hydroxyl groups attached to aromatic fragments with *o*-phos-

Table 2
Selected bond distances and angles of **2a**, **3a** and **3b** (data for one of the two unique molecules of **3b** is listed, labels for isostructural atoms for **3b** are given in parentheses)

Bond distances (Å)	2a	3a	3b
P1–C1 (P11–C11)	1.8435(14)	1.813(2)	1.833(2)
C1–C2 (C11–C12)	1.3930(19)	1.385(3)	1.388(3)
C3–O3 (C13–O13)	1.3548(16)	1.353(2)	1.353(2)
P1–O1 (P11–O11)		1.4936(16)	1.5002(17)
Bond angles (°)			
P1–C1–C2 (P11–C11–C12)	126.99(10)	122.66(14)	124.07(16)
C1–C2–F2 (C11–C12–F12)	119.42(12)	118.08(17)	118.50(18)
O3–C3–C2 (O13–C13–C12)	120.36(12)	118.09(17)	118.17(19)
C1–C2–C3 (C11–C12–C13)	122.82(12)	124.86(17)	124.81(19)
O1–P1–C1 (O11–P11–C11)		107.05(9)	106.92(10)

Table 1
Summary of crystallographic data for **2a** and **3a**–**b**

Compound	2a · $2C_5H_5N$	3a	3b
Formula	$C_{40}H_{32}F_2N_2O_2P_2$	$C_{30}H_{22}F_2O_4P_2$	$C_{18}H_{30}F_2O_4P_2$
Formula weight	672.62	546.42	410.36
Space group	$P21/n$	$P\bar{1}$	$P\bar{1}$
a (Å)	13.0046(19)	8.747(5)	7.5409(9)
b (Å)	9.4524(14)	8.824(5)	11.243(2)
c (Å)	14.216(2)	9.375(5)	14.178(2)
α (°)	90	74.732(5)	69.56(2)
β (°)	99.791(2)	75.109(5)	74.96(1)
γ (°)	90	71.469(5)	89.64(1)
V (Å^3)	1722.0(4)	649.9(6)	1083.0(3)
Z	2	2	2
ρ_{calc} (g/cm^3)	1.297	1.396	1.258
μ (Mo Kα, mm^{-1})	0.175	0.217	0.236
T (K)	243.0(2)	293(2)	293(2)
λ (Å)	0.71073	0.71069	0.71073
θ Range (°)	1.96–32.03	2.29–22.47	1.59–22.47
Measured/independent reflections	5991	1553	2469
Final R indices [$I > 2\sigma(I)$][a]	R_1 = 0.0556, wR_2[b] = 0.1590	R_1 = 0.0295, wR_2[c] = 0.0787	R_1 = 0.034, wR_2[d] = 0.093
R indices (all data)	R_1 = 0.0786, wR_2 = 0.1788	R_1 = 0.0329, wR_2 = 0.0817	R_1 = 0.041; wR_2 = 0.098
Largest difference in peak and hole	0.430, −0.318	0.143, −0.214	0.253, −0.285
Goodness-of-fit on F^2	1.060	1.061	1.064

[a] $R_1 = \Sigma||Fo| - |Fc||/\Sigma|Fo|$.
[b] $wR_2 = [\sum[w(F_o^2 - F_c)^2]/\sum[w(F_o^2)^2]]^{1/2}$, where $w = 1/[\sigma^2(F_o^2) + (0.0900P)^2 + 0.3145P]$ and $P = 1/3\max(0, F_o^2) + 2/3F_c^2$.
[c] $w = 1/[\sigma^2(F_o^2) + (0.0411P)^2 + 0.2412P]$.
[d] $w = 1/[\sigma^2(F_o^2) + (0.0553P)^2 + 0.4283P]$.

Table 3
Selected bond distances and angles of **2a**, **2aH**, **3a** and **3aH** structures calculated at B3LYP/6-31G(d) level of theory

Bond distances (Å)	**2a**		**3a**	
	Calculated	X-ray	Calculated	X-ray
P1–C1	1.86	1.8435(14)	1.83	1.813(2)
C1–C2	1.39	1.3930(19)	1.39	1.385(3)
C3–O3	1.36	1.3548(16)	1.34	1.353(2)
P1–O1			1.52	1.4936(16)
Bond angles (°)				
P1–C1–C2	126.9	126.99(10)	122.6	122.66(14)
C1–C2–F2	120.5	119.42(12)	118.7	118.08(17)
O3–C3–C2	120.1	120.36(12)	117.7	118.09(17)
C1–C2–C3	120.9	122.82(12)	124.4	124.86(17)
O1–P1–C1			108.0	107.05(9)
	2aH		**3aH**	
P1–C1	1.85		1.82	
C1–C2	1.40		1.40	
C3–O3	1.37		1.35	
P1–O1			1.52	
Bond angles (°)				
P1–C1–C2	124.4		121.7	
C1–C2–F(H)2	119.3		120.8	
O3–C3–C2	121.9		117.5	
C1–C2–C3	121.6		122.0	
O1–P1–C1			109.8	

Table 4
Frontier orbitals of **2a** and their compositions calculated at B3LYP/TZVP//B3LYP/6-31G(d) level of theory

		HOMO(−1)	HOMO	LUMO	LUMO(+1)
Energy (eV)		−6.20	−5.98	−1.56	−1.07
C, H atoms on Ph rings	Pop. (%)	48.2	31.1	26.7	81.6
s	Orbitals:	1.4	1.5	2.6	0.0
p	Orbitals:	46.0	29.2	23.5	79.9
d	Orbitals:	0.8	0.5	0.6	2.0
P atoms	Pop. (%)	45.5	32.1	11.8	12.4
s	Orbitals:	8.7	6.0	0.0	0.0
p	Orbitals:	36.6	25.9	7.9	10.4
d	Orbitals:	0.2	0.2	3.9	2.1
F atoms	Pop. (%)	0.1	0.5	1.2	0.1
s	Orbitals:	0.0	0.0	0.0	0.0
p	Orbitals:	0.1	0.5	1.2	0.4
d	Orbitals:	0.0	0.0	0.0	0.0
OH group atoms	Pop. (%)	0.4	9.7	0.9	0.5
s	Orbitals:	0.1	0.2	0.0	0.0
p	Orbitals:	0.3	9.6	0.8	0.5
d	Orbitals:	0.0	0.0	0.0	0.0
C atoms on inner ring	Pop. (%)	5.8	26.5	59.4	5.4
s	Orbitals:	1.3	0.2	0.0	4.9
p	Orbitals:	4.3	25.7	57.7	0.1
d	Orbitals:	0.2	0.6	1.7	0.4

phinyl/phosphoryl substituents [62,65]. The other bond distances and angles (Table 2) are unexceptional.

3.3. Electrochemistry

The redox activities of compounds **2a**–**b** and **3a**–**b** were investigated by cyclic voltammetry. CV profiles of compounds **2a**/**2b** and **3a**/**3b** are very similar, thus only the data for **2a** and **3a** is presented and discussed.

The cyclic voltammogram of **2a** contains broad irreversible waves in the oxidative scan (Fig. 4, left). Such a profile is most likely dictated by chemical reactions which accompany the oxidation process. Simple *p*-quinones are well known to react with tertiary phosphines, forming (irreversibly) zwitterionic adducts (Eq. (3)) [22]. Therefore, an oxidation of the central hydroquinone cores in **2a**–**b** into quinones is most likely accompanied by the immediate addition of a $-PR_2$ group from another **2a**–**b** molecule, producing complex adducts.

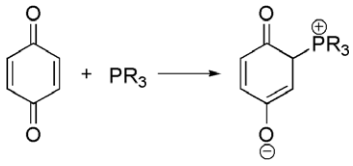

(3)

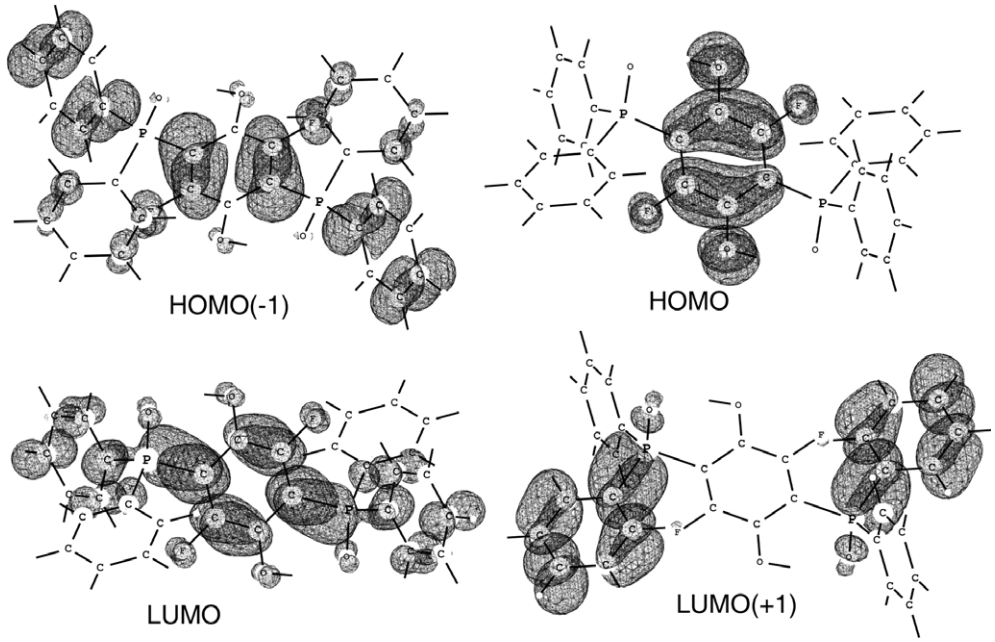

Fig. 6. Frontier orbitals (contour plots) of **3a**.

A cyclic voltammogram for hydroquinone **3a** displays an irreversible peak at 0.96 V, which is associated with a peak at 0.55 V on the return scan (Fig. 4, right). The non-reversibility of the oxidation process here is most likely caused by the coupling of electron/proton transfers during the oxidation process. The nature of the hydroquinone/quinone oxidation ($2e^-/2H^+$ transfer in one step or two successive $1e^-/1H^+$ transfers) is well known to be proton-dependant [66]. The hydroxylic protons in **3a**–**b** are engaged in strong hydrogen bonding with the adjacent P═O oxygens (as seen in X-ray structures), thus the H^+ transfer associated with the oxidation of the hydroquinone moiety will be directly influenced by this interaction. Similar CV profiles were reported for hydroquinones where proton-accepting (amine, carboxylate) substituents are present on the quinone moiety [15,67].

Table 5
Frontier orbitals of **3a** and their compositions calculated at B3LYP/TZVP//B3LYP/6-31G(d) level of theory

		HOMO(−1)	HOMO	LUMO	LUMO(+1)
Energy (eV)		−7.33	−5.89	−1.84	−1.36
C, H atoms on Ph rings	Pop. (%)	55.6	0.6	28.4	84.3
s	Orbitals:	0.3	0.1	0.0	0.2
p	Orbitals:	54.7	0.5	28.2	82.0
d	Orbitals:	0.6	0.0	0.7	2.0
P═O atoms	Pop. (%)	1.4	0.2	17.4	12.7
s	Orbitals:	0.0	0.0	0.2	0.0
p	Orbitals:	0.7	-0.1	12.5	9.7
d	Orbitals:	0.6	0.2	4.7	3.8
F atoms	Pop. (%)	3.9	4.6	1.3	0.0
s	Orbitals:	0.0	0.0	0.0	0.0
p	Orbitals:	3.9	4.6	1.3	0.0
d	Orbitals:	0.0	0.0	0.0	0.0
OH group atoms	Pop. (%)	0.9	32.0	1.4	0.9
s	Orbitals:	0.0	0.0	0.1	0.8
p	Orbitals:	0.9	32.0	1.3	0.1
d	Orbitals:	0.0	0.0	0.0	0.0
C atoms on inner ring	Pop. (%)	38.2	62.6	51.6	2.2
s	Orbitals:	0.1	0.1	0.0	0.0
p	Orbitals:	37.6	61.1	50.1	2.7
d	Orbitals:	0.5	1.5	1.5	0.1

3.4. Calculations

3.4.1. Structural parameters and calculated frontier molecular orbitals (FMOs)

The selected structural parameters of **2a** and **3a** structures optimized at B3LYP/6-31G(d) level of theory are shown in Table 3. Calculated structural parameters of **2a** and **3a** are compared with the X-ray structural data. The calculated geometries of **2a** and **3a** agree with the experimentally obtained ones well within 2.7% error (Table 3). Fluorine-free analogs of **2a** and **3a** (**2aH** and **3aH**) were also examined in order to estimate the effects of fluorine substitution on the structural and electronic properties. The calculated structural parameters of **2aH** and **3aH** are also presented in Table 3.

The frontier orbitals of **2a** and **3a** calculated at B3LYP/TZVP//B3LYP/6-31G(d) level of theory are shown in Figs. 5 and 6 with corresponding orbital composition shown in Tables 4 and 5, respectively. In **2a** the electron density of the HOMO is localized on the electron rich inner ring, Ph rings, P atoms and OH centers (Table 4). The latter two localize HOMO electron density mainly in p-orbitals (25.9% and 9.6% of all HOMO density) and these atoms can be involved in metal ion coordination by donating electrons into readily available d-orbitals. This agrees well with the ligating properties of **2a** reported in this paper.

Remarkably, the HOMO on **3a** is located preferably on the central ring carbon atoms, OH groups and F atoms (Table 5). Thus, based on the electron distribution only in the HOMO it appears that the coordination of metal ions to **3a** would occur preferentially at rather unusual [O,F] pockets and not at [O,(O═P)]. However, the ligation at the later site can not be excluded, as the oxygen atom in the P═O functionality contributes significantly to

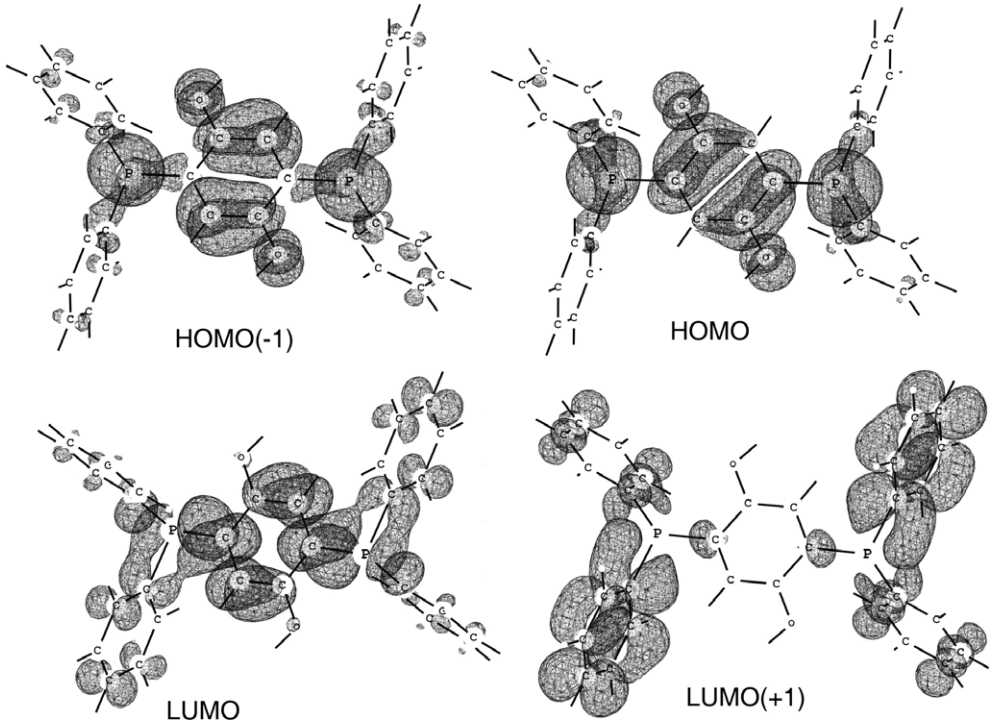

Fig. 7. Frontier orbitals (contour plots) of **2aH**.

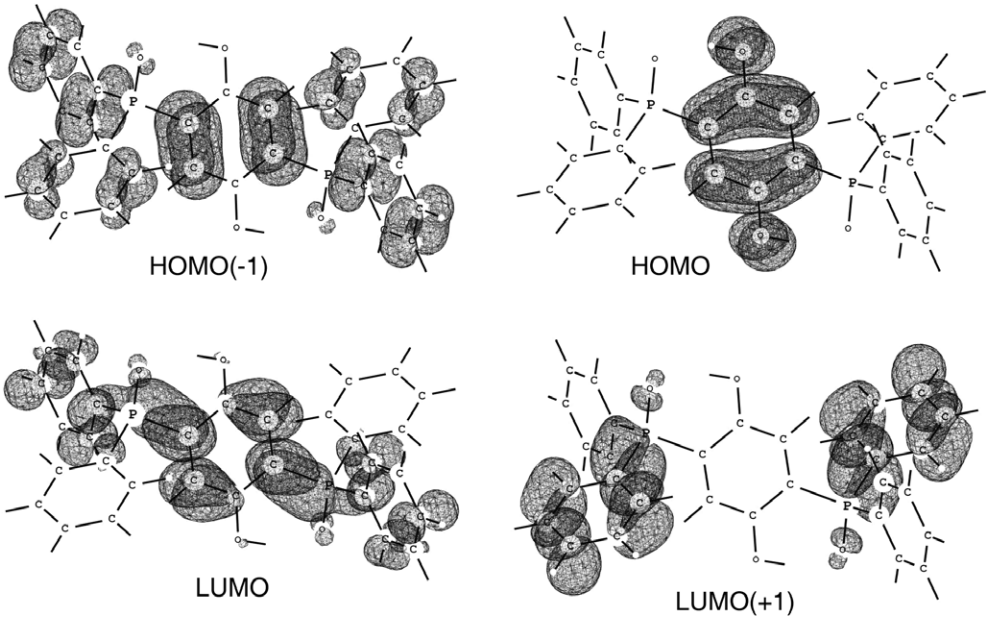

Fig. 8. Frontier orbitals (contour plots) of **3aH**.

Table 6
Frontier orbitals of **2aH** and their compositions calculated at B3LYP/TZVP//B3LYP/6-31G(d) level of theory

		HOMO(−1)	HOMO	LUMO	LUMO(+1)
Energy (eV)		−6.16	−5.56	−1.06	−0.94
C, H atoms on Ph rings	Pop. (%)	17.4	14.2	30.8	89.6
s	Orbitals:	0.9	2.2	2.9	0.3
p	Orbitals:	16.2	11.8	27.1	87.2
d	Orbitals:	0.3	0.3	0.8	2.1
P atoms	Pop. (%)	22.8	26.1	12.4	7.4
s	Orbitals:	4.6	4.7	0.3	0.1
p	Orbitals:	18.1	21.0	9.0	5.0
d	Orbitals:	0.1	0.4	3.1	2.3
H atoms	Pop. (%)	0.4	0.1	0.2	0.2
s	Orbitals:	0.2	0.1	0.0	0.2
p	Orbitals:	0.2	0.0	0.2	0.0
d	Orbitals:	0.4	0.1	0.2	0.2
OH group atoms	Pop. (%)	15.1	13.8	0.5	0.0
s	Orbitals:	0.0	0.0	0.0	-0.1
p	Orbitals:	15.0	13.8	0.5	0.1
d	Orbitals:	0.0	0.0	0.0	0.0
C atoms on inner ring	Pop. (%)	44.5	45.8	56.1	2.9
s	Orbitals:	0.3	0.3	-0.1	0.1
p	Orbitals:	43.3	44.7	54.8	2.6
d	Orbitals:	0.8	0.9	1.4	0.1

Table 7
Frontier orbitals of **3aH** and their compositions calculated at B3LYP/TZVP//B3LYP/6-31G(d) level of theory

		HOMO(−1)	HOMO	LUMO	LUMO(+1)
Energy (eV)		−7.26	−5.71	−1.72	−1.38
C, H atoms on Ph rings	Pop. (%)	57.5	1.2	32.7	85.4
s	Orbitals:	0.2	0.0	0.3	0.6
p	Orbitals:	56.7	1.3	31.6	82.7
d	Orbitals:	0.6	0.0	0.8	2.0
P═O atoms	Pop. (%)	1.7	0.5	15.0	11.1
s	Orbitals:	0.0	0.0	0.1	0.0
p	Orbitals:	1.2	0.0	10.5	8.4
d	Orbitals:	0.5	0.4	4.4	3.4
H atoms	Pop. (%)	0.1	0.1	0.3	0.1
s	Orbitals:	0.0	0.0	0.1	0.1
p	Orbitals:	0.1	0.1	0.2	0.0
d	Orbitals:	0.0	0.0	0.0	0.0
OH group atoms	Pop. (%)	0.0	33.2	0.5	0.4
s	Orbitals:	0.0	0.0	0.1	0.3
p	Orbitals:	0.0	33.2	0.4	0.1
d	Orbitals:	0.0	0.0	0.0	0.0
C atoms on inner ring	Pop. (%)	40.7	64.9	51.5	3.1
s	Orbitals:	0.1	0.0	0.2	0.0
p	Orbitals:	40.2	63.5	50.0	3.8
d	Orbitals:	0.4	1.4	1.3	0.1

the composition of the LUMO and can function as an acceptor ligand.

3.4.2. Effect of fluorine atoms on the stability of the compounds

To investigate any increased stability of **2a** and **3a** we performed DFT calculations using hydrogens instead of fluorine atoms on the central ring (compounds **2aH** and **3aH**). Frontier orbitals of **2aH** and **3aH** calculated at B3LYP/TZVP//B3LYP/6-31G(d) level of theory are shown in Figs. 7 and 8 with corresponding orbital composition shown in Tables 6 and 7, respectively.

The calculated energies of the HOMO and the LUMO orbitals in **2a** and **2aH** are −5.98 and −1.56 eV and −5.56 and −1.06 eV, respectively (Tables 4 and 6, respectively) with the HOMO–LUMO gaps at 4.42 and 4.5 eV. While the HOMO–LUMO gap decreases with fluorination by 0.08 eV, the HOMO and the LUMO orbital energies are lower in the fluorinated compounds by 0.42 and 0.5 eV, respectively. Thus, the presence of highly electronegative fluorine atom clearly stabilizes the HOMO and the LUMO levels in **2a** rendering it more stable than the unfluorinated counterpart **2aH**. Similarly, the HOMO and LUMO energies of **3a** and **3aH** are −5.98 and −1.84 eV and −5.71 and −1.72 eV, respectively (Tables 5 and 7). Here the HOMO and LUMO orbitals in fluorinated compounds are shifted by 0.27 and 0.12 eV towards lower energy values with the HOMO–LUMO gap increasing with fluorination by 0.15 eV. Such batho- and hypsochromic shifts in fluorinated π-conjugated organic molecules have previously been attributed to an interplay between inductive and mesomeric effects of fluorine atoms on the specific molecular backbone [68].

A comparison of the occupied orbitals also provides insights into the stability of **2a** and **3a** as compared with unfluorinated compounds **2aH** and **3aH**. HOMO in **2a** has 31.1% of total electron density located on Ph rings (Fig. 4 and Table 4), whereas only 14.2% is located in **2aH** (Fig. 5 and Table 5). The orbitals involved are predominantly p-type, and there is strong electron delocalization between the fluorine atoms, the inner ring, the phosphorus atoms and the phenyl carbons in **2a**, but not in **2aH**. In **3a** and **3aH** case this effect is less pronounced and primarily HOMO(−1) orbitals are involved into the interactions of inner ring with phosphorus atoms as well as Ph groups.

4. Conclusion

Compounds containing 2,5-bis(phosphine)- and 2,5-(bis)phosphinyl-*p*-hydroquinone motifs can be conveniently synthesized. They represent a relatively unexplored class of noninnocent binucleating ligands, which should be suitable for the construction of highly linear polymetallic assemblies. The electronic properties of the ligands are shown to be sensitive to the nature of the substituents at the remaining two positions on the hydroquinone ring, thus numerous opportunities for tuning the structure-property relations exist.

Supplementary material

CCDC 687861, 681176 and 682455 contains the supplementary crystallographic data for **2a**, **3a** and **3b**. These data can be obtained free of charge from The Cambridge Crystallographic Data Centre via www.ccdc.cam.ac.uk/data_request/cif.

Acknowledgment

Support by Michigan Technological University is acknowledged.

References

[1] R.R. Burch, Chem. Mater. 2 (1990) 633.
[2] J.M. Tanski, T.P. Vaid, E.B. Lobkovsky, P.T. Wolczanski, Inorg. Chem. 39 (2000) 4756.
[3] J.M. Tanski, P.T. Wolczanski, Inorg. Chem. 40 (2001) 346.
[4] T.P. Vaid, E.B. Lobkovsky, P.T. Wolczanski, J. Am. Chem. Soc. 119 (1997) 8742.
[5] T.P. Vaid, J.M. Tanski, J.M. Pette, E.B. Lobkovsky, P.T. Wolczanski, Inorg. Chem. 38 (1999) 3394.
[6] M.S. Thorum, M.L. Taliaferro, K.S. Min, J.S. Miller, Polyhedron 26 (2007) 2247.
[7] H. Matsui, R. Kudo, T. Ishikawa, M. Yoshihara, J. Mater. Sci. 48 (2005) 4917.
[8] M. Oh, G.B. Carpenter, D.A. Sweigart, Acc. Chem. Res. 37 (2004) 1.
[9] J.A. Reingold, S.U. Son, G.B. Carpenter, D.A. Sweigart, J. Inorg. Organomet. Polym. Mater. 16 (2006) 1.
[10] J.A. Reingold, S.U. Son, S.B. Kim, C.A. Dullaghan, M. Oh, P.C. Frake, G.B. Carpenter, D.A. Sweigart, Dalton Trans. (2006) 2385.
[11] J. Moussa, H. Amouri, Angew. Chem., Int. Ed. 47 (2008) 1372.
[12] S. Kitagawa, S. Kawata, Coord. Chem. Rev. 224 (2002) 11.
[13] R. Dinnebier, H.-W. Lerner, L. Ding, K. Shankland, W.I.F. David, P.W. Stephens, M. Wagner, Z. Anorg. Allg. Chem. 628 (2002) 310.
[14] G. Margraf, T. Kretz, F.F.D. Biani, F. Laschi, S. Losi, P. Zanello, J.W. Bats, B. Wolf, K. Removic-Langer, M. Lang, A. Prokofiev, W. Assmus, H.-W. Lerner, M. Wagner, Inorg. Chem. 45 (2006) 1277.
[15] T. Kretz, J.W. Bats, S. Losi, B. Wolf, H.-W. Lerner, M. Lang, P. Zanello, M. Wagner, Dalton Trans. (2006) 4914.
[16] A.V. Prokofiev, E. Dahlmann, F. Ritter, W. Assmus, G. Margraf, M. Wagner, Cryst. Res. Technol. 39 (2004) 1014.
[17] B. Wolf, A. Bruhl, V. Pashchenko, K. Removic-Langer, T. Kretz, J.W. Bats, H.W. Lerner, M. Wagner, A. Salguero, T. Saha-Dasgupta, B. Rahaman, R. Valenti, M. Lang, C.R. Chim. 10 (2007) 109.
[18] B. Wolf, S. Zherlitsyn, B. Luthi, N. Harrison, U. Low, V. Pashchenko, M. Lang, G. Margraf, H.W. Lerner, E. Dahlmann, F. Ritter, W. Assmus, M. Wagner, Phys. Rev. B 69 (2004).
[19] S. Scheuermann, T. Kretz, H. Vitze, J.W. Bats, M. Bolte, H.W. Lerner, M. Wagner, Chem. Eur. J. 14 (2008) 2590.
[20] S. Ernst, P. Hänel, J. Jordanov, W. Kaim, V. Kasack, E. Roth, J. Am. Chem. Soc. 111 (1989) 1733.
[21] S.B. Sembiring, S.B. Colbran, D.C. Craig, Inorg. Chem. 34 (1995) 761.
[22] F. Ramirez, S. Dershowitz, J. Am. Chem. Soc. 78 (1956) 5614.
[23] S.B. Colbran, D.C. Craig, S.B. Sembiring, Inorg. Chim. Acta 176 (1990) 225.
[24] S.B. Sembiring, S.B. Colbran, R. Bishop, D.C. Craig, A.D. Rae, Inorg. Chim. Acta 228 (1995) 109.
[25] S.B. Sembiring, S.B. Colbran, D.C. Craig, J. Chem. Soc., Dalton Trans. (1999) 1543.
[26] S.B. Sembiring, S.B. Colbran, L.R. Hanton, Inorg. Chim. Acta 202 (1992) 67.
[27] I. Manners, Synthetic Metal-Containing Polymers, Wiley-VCH, Weinheim, 2004.
[28] K.A. Williams, A.J. Boydston, C.W. Bielawski, Chem. Soc. Rev. 36 (2007) 729–744.
[29] B.J. Holliday, T.M. Swager, Chem. Commun. (2005) 23.
[30] J.A. McCleverty, M.D. Ward, Acc. Chem. Res. 31 (1998) 842.
[31] M.D. Ward, J. Solid State Electrochem. 9 (2005) 778.
[32] M.D. Ward, J.A. McCleverty, J. Chem. Soc., Dalton Trans (2002) 275.
[33] A. Dei, D. Gatteschi, C. Sangregorio, L. Sorace, Acc. Chem. Res. 37 (2004) 827.
[34] P.L. Coe, A.J. Waring, T.D. Yarwood, J. Chem. Soc. Perkin Trans. 1 (1995) 2729.
[35] O. Dahl, Acta Chem. Scand. 23 (1969) 2342.
[36] J. Heinicke, N. Peulecke, M.K. Kindermann, P.G. Jones, Z. Anorg. Allg. Chem. 631 (2005) 67.
[37] R.H. Blessing, Acta Crystallogr. Sect. A 51 (1995) 33.
[38] Bruker Analytical X-ray Systems, Madison, WI, 2005.
[39] A. Altomare, M.C. Burla, M. Camalli, G.L. Cascarano, C. Giacovazzo, A. Guagliardi, A.G.G. Moliterni, G. Polidori, R. Spagna, J. Appl. Crystallogr. 32 (1999) 115.
[40] Bruker Analytical X-ray Systems, Madison, WI, 2000.
[41] N. Kongprakaiwoot, M.S. Bultman, R.L. Luck, E. Urnezius, Inorg. Chim. Acta 358 (2005) 3423.
[42] M.J. Frisch, G.W. Trucks, H.B. Schlegel, G.E. Scuseria, M.A. Robb, J.R. Cheeseman, J.A. Montgomery Jr., T. Vreven, K.N. Kudin, J.C. Burant, J.M. Millam, S.S. Iyengar, J. Tomasi, V. Barone, B. Mennucci, M. Cossi, G. Scalmani, N. Rega, G.A. Petersson, H. Nakatsuji, M. Hada, M. Ehara, K. Toyota, R. Fukuda, J. Hasegawa, M. Ishida, T. Nakajima, Y. Honda, O. Kitao, H. Nakai, M. Klene, X. Li, J.E. Knox, H.P. Hratchian, J.B. Cross, V. Bakken, C. Adamo, J. Jaramillo, R. Gomperts, R.E. Stratmann, O. Yazyev, A.J. Austin, R. Cammi, C. Pomelli, J.W. Ochterski, P.Y. Ayala, K. Morokuma, G.A. Voth, P. Salvador, J.J. Dannenberg, V.G. Zakrzewski, S. Dapprich, A. D. Daniels, M.C. Strain, O. Farkas, D.K. Malick, A.D. Rabuck, K. Raghavachari, J.B. Foresman, J.V. Ortiz, Q. Cui, A.G. Baboul, S. Clifford, J. Cioslowski, B.B. Stefanov, G. Liu, A. Liashenko, P. Piskorz, I. Komaromi, R.L. Martin, D.J. Fox, T. Keith, M.A. Al-Laham, C.Y. Peng, A. Nanayakkara, M. Challacombe, P.M. W. Gill, B. Johnson, W. Chen, M.W. Wong, C. Gonzalez, J.A. Pople, Gaussian Inc., Wallingford, CT, 2004.
[43] C.T. Lee, W.T. Yang, R.G. Parr, Phys. Rev. B 37 (1988) 785.
[44] A.D. Becke, J. Chem. Phys. 98 (1993) 5648.
[45] A. Schafer, C. Huber, R. Ahlrichs, J. Chem. Phys. 100 (1994) 5829.
[46] S.I. Gorelsky, University of Ottawa, Ottawa, 2007.
[47] S.I. Gorelsky, A.B.P. Lever, J. Organomet. Chem. 635 (2001) 187.
[48] R.S. Mulliken, J. Chem. Phys. 23 (1955) 1833.
[49] R.S. Mulliken, J. Chem. Phys. 23 (1955) 1841.
[50] R.S. Mulliken, J. Chem. Phys. 23 (1955) 2338.
[51] R.S. Mulliken, J. Chem. Phys. 23 (1955) 2343.
[52] G.A. Zhurko. http://www.chemcraftprog.com, 2004–2008.
[53] N. Kongprakaiwoot, R.L. Luck, E. Urnezius, J. Organomet. Chem. 689 (2004) 3350.
[54] N. Kongprakaiwoot, R.L. Luck, E. Urnezius, J. Organomet. Chem. 691 (2006) 5024.
[55] G.P. Crowther, R.J. Sundberg, A.M. Sarpeshkar, J. Org. Chem. 49 (1984) 4657.
[56] L. Horner, G. Simons, Phosphorus, Sulfur Silicon Relat. Elem. 14 (1983) 189.
[57] A. Suarez, M.A. Mendez-Rojas, A. Pizzano, Organometallics 21 (2002) 4611.
[58] J.S. Kim, A. Sen, I.A. Guzei, L.M. Liable-Sands, A.L. Rheingold, J. Chem. Soc., Dalton Trans. (2002) 4726.
[59] K. Saatchi, B.O. Patrick, C. Orvig, Dalton Trans. (2005) 2268.
[60] J. Heinicke, M. He, A. Dal, H.-F. Klein, O. Hetche, W. Keim, U. Flörke, H.-J. Haupt, Eur. J. Inorg. Chem. 2000 (2000) 431.
[61] J. Heinicke, R. Kadyrov, M.K. Kindermann, M. Koesling, P.G. Jones, Chem. Ber. 129 (1996) 1547.
[62] A. Beganskiene, N.I. Nikishkin, R.L. Luck, E. Urnezius, Heteroat. Chem. 17 (2006) 656.
[63] D.R. Joyce, E.M.A. Gijzen, G.C. Davis, Polym. Prepr. 44 (2003) 751.
[64] L. Pauling. The Nature of the Chemical Bond and the Structure of Molecules and Crystals; An Introduction to Modern Structural Chemistry; Cornell University Press, Ithaca, NY, 1960.
[65] K. Kobiro, M. Shi, Y. Inoue, Chem. Lett. 28 (1999) 633.
[66] M. Quan, D. Sanchez, M.F. Wasylkiw, D.K. Smith, J. Am. Chem. Soc. 129 (2007) 12847.
[67] C. Costentin, M. Robert, J.M. Saveant, J. Am. Chem. Soc. 128 (2006) 8726.
[68] B.M. Medina, D. Beljonne, H.J. Egelhaaf, J. Gierschner, J. Chem. Phys. 126 (2007) 111101.